Journal of
Marine Science and Engineering

MDPI

Article

The Impact of Special Marine Environments Such as the Kuroshio on Hydroacoustic Detection Equipment

Xueqin Zhang [1,2], Kunde Yang [1,2,3] and Xiaolin Yu [4,*]

1 School of Marine Science and Technology, Northwestern Polytechnical University, Xi'an 710072, China; zhangxueqin1984@mail.nwpu.edu.cn (X.Z.); ykdzym@nwpu.edu.cn (K.Y.)
2 Key Laboratory of Ocean Acoustic and Sensing, Ministry of Industry and Information Technology, Northwestern Polytechnical University, Xi'an 710072, China
3 Ocean Institute, Northwestern Polytechnical University, Suzhou 215400, China
4 Shanghai Acoustics Laboratory, Chinese Academy of Sciences, Shanghai 201815, China
* Correspondence: yuxiaolin@mail.ioa.ac.cn

Abstract: In order to study the impact of acoustic propagation characteristics in the northeastern South China Sea, GEBCO08 global terrain grid data and Argo data were used to numerically simulate the acoustic transmission characteristics of two stations in the northeast South China Sea affected by the Kuroshio. The impact of different marine environments on acoustic transmission characteristics was analyzed. The results show that increasing the deployment depth of a sound source within a certain range will reduce the transmission loss; deploying a sound source near the axis of the surface acoustic channel or the deep-sea acoustic channel will also greatly increase the propagation distance of sound signals; and the presence of topography such as undersea mountains will increase the transmission loss.

Keywords: marine environments; acoustic transmission; topography

Citation: Zhang, X.; Yang, K.; Yu, X. The Impact of Special Marine Environments Such as the Kuroshio on Hydroacoustic Detection Equipment. *J. Mar. Sci. Eng.* **2024**, *12*, 1594. https://doi.org/10.3390/jmse12091594

Academic Editor: Rouseff Daniel

Received: 7 August 2024
Revised: 5 September 2024
Accepted: 7 September 2024
Published: 9 September 2024

1. Introduction

Due to the transmission loss of light waves and electromagnetic waves in water being very large, sound waves are the most effective information carriers in the field of acoustic detection, navigation, and communication. Sonar and other acoustic devices serve as crucial detection and navigation instruments for vessels, but the quality of the underwater acoustic environment will directly affect their ability to obtain underwater information [1]. The marine acoustic environment is extremely complex and variable, with various nonuniformities in the seawater medium and its boundaries that can have a strong impact on oceanic sound transmission [2]. Studying the acoustic propagation characteristics in complex marine environments and making timely predictions that meet the requirements is of great significance for the detection of hydroacoustic detection equipment.

The Kuroshio [3,4] originates from the North Equatorial Current and is the main western boundary current of the North Pacific [5]. It flows northward along the eastern coast of the Philippines, and when it passes through the Luzon Strait, it often bends clockwise due to a deep gap of over 300 km in the strait, invading the northeast part of the South China Sea [6,7]. The high-temperature and high-salinity Pacific water carried by the Kuroshio has a significant impact on the heat–salt balance, energy, and eddy activities in the northeast part of the South China Sea after its entry [8,9]. Influenced by the Kuroshio, the marine environment in the South China Sea exhibits complex characteristics that have important implications for the application of hydroacoustic detection equipment [2].

In this article, we study the acoustic propagation characteristics in the northeastern South China Sea and analyze the impact of different marine environments on acoustic propagation.

2. Marine Environmental Parameters

In this paper, two stations in the northeastern part of the South China Sea—O1 (19.6° N, 115.6° E) and O2 (18.2° N, 117.5° E)—were selected, and four acoustic survey lines in different directions were chosen for each station (O1-S1, O1-S2, O1-S3, O1-S4, O2-T1, O2-T2, O2-T3, and O2-T4). The locations of the stations and the acoustic survey lines are shown in Figure 1.

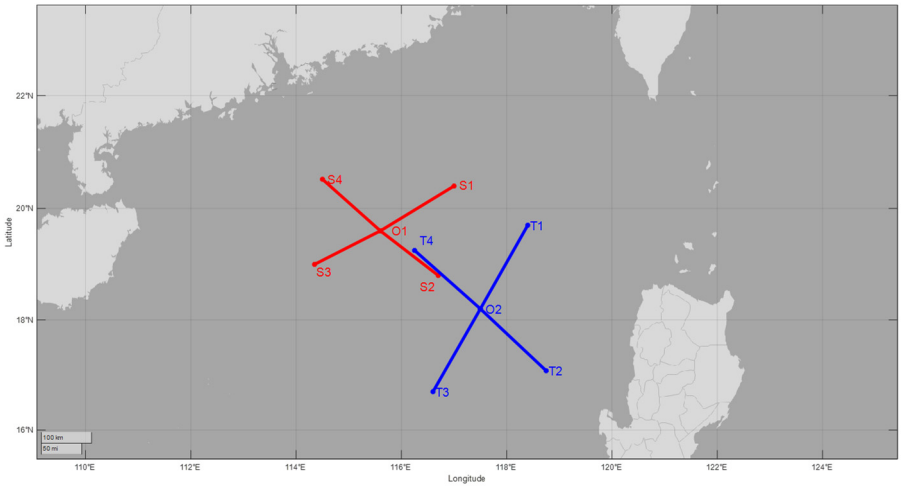

Figure 1. Locations of the stations and acoustic survey lines employed in this study.

The bathymetric data are from the GEBCO_08 global topographic gridded dataset [10,11], which has a resolution of 30 arc minutes and is publicly available. The vast majority of the GEBCO_08 ocean depth data are measured by quality-controlled shipboard sounders, and the data between the measurement points are interpolated by satellite gravity data corrections. Satellite gravity data provide measurements of Earth's gravity field, which can be used to infer Earth's mass distribution and topographic features. However, due to the nature of satellite gravity data, it may not be possible to obtain accurate elevation information for each site. Therefore, the elevation of unknown sites is estimated using the topographic data detected by existing shipborne sounders as a baseline, combining these data with satellite gravity data, and using interpolation algorithms (such as kriging interpolation or bilinear interpolation). In this way, a global terrain mesh dataset can be obtained, which fuses information from multiple data sources to obtain a continuous toposurface through interpolation techniques.

Acoustic survey line O1-S1 is northeast-trending, and the water depth changes from 1800 m to 500 m in the distance range of 0–150 km. Acoustic survey line O1-S2 is southeast-trending, and the water depth changes from 1800 to 3500 m in the distance range of 0–150 km. Acoustic survey line O1-S3 is southwest-trending, and the water depth changes from 1800 to 2300 m in the distance range of 0–30 km, then from 2300 to 1300 m in the distance range of 30–110 km, and then the terrain is relatively flat. And lastly, acoustic survey line O1-S4 is northwest trending, which is a typical continental slope terrain, and the water depth changes from 1800 m to 150 m in the distance range of 0–80 km, and then the terrain is relatively flat. The variation in water depth of the four acoustic survey lines is shown in Figure 2.

Acoustic survey line O2-T1 is northeast-trending, and the seabed terrain changes little, on the whole, with an average water depth of about 3900 m. Acoustic survey line O2-T2 is southeast-trending, and the water depth changes little, on the whole, in the range of 0–125 km, with an average water depth of about 4000 m, but a seamount appears after 130 km, and the water depth gradually becomes shallow, changing to 500 m at 170 km. Acoustic survey line O2-T3 is southwest-trending, and the seabed terrain is relatively flat within 60 km from the O2 station, with an average water depth of about 4000 m, after which

it crosses a seamount area whose highest point is about 80 km from station O2, with a water depth of 2100 m, and then, after 90 km the terrain is flat, with an average water depth of about 4000 m. And lastly, acoustic survey line O2-T4 is northwest-trending, and the terrain changes little in the range of 0–100 km, with an average water depth of about 4000 m, and then, the water depth changes from 4000 m to 2000 m in the range of 100–180 km. The variation in water depth of these four acoustic lines is shown in Figure 3.

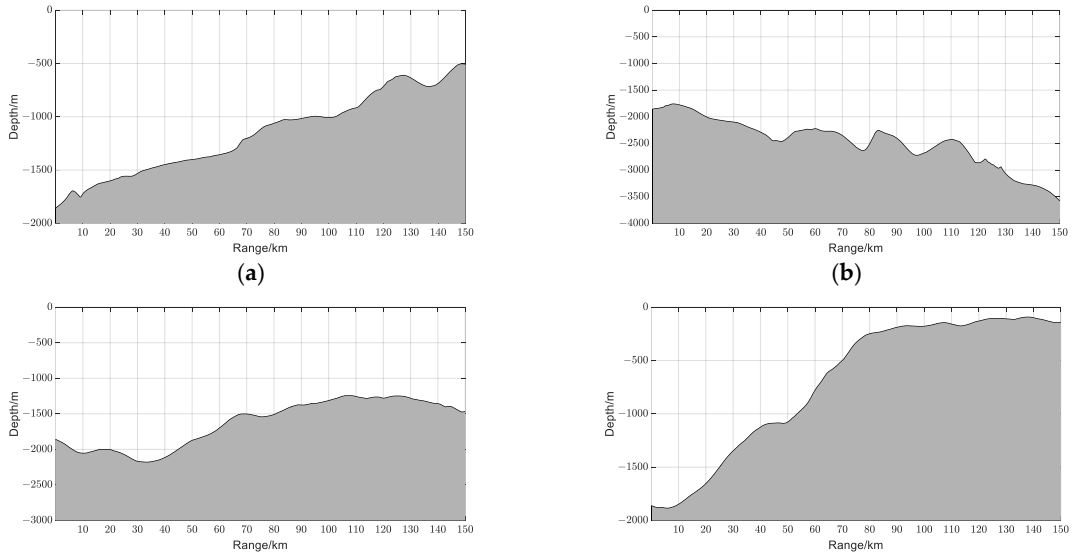

Figure 2. Water depth variation of the four acoustic survey lines at station O1. (**a**) Change in water depth of acoustic survey line O1-S1; (**b**) Change in water depth of acoustic survey line O1-S2; (**c**) Change in water depth of acoustic survey line O1-S3; (**d**) Change in water depth of acoustic survey line O1-S4.

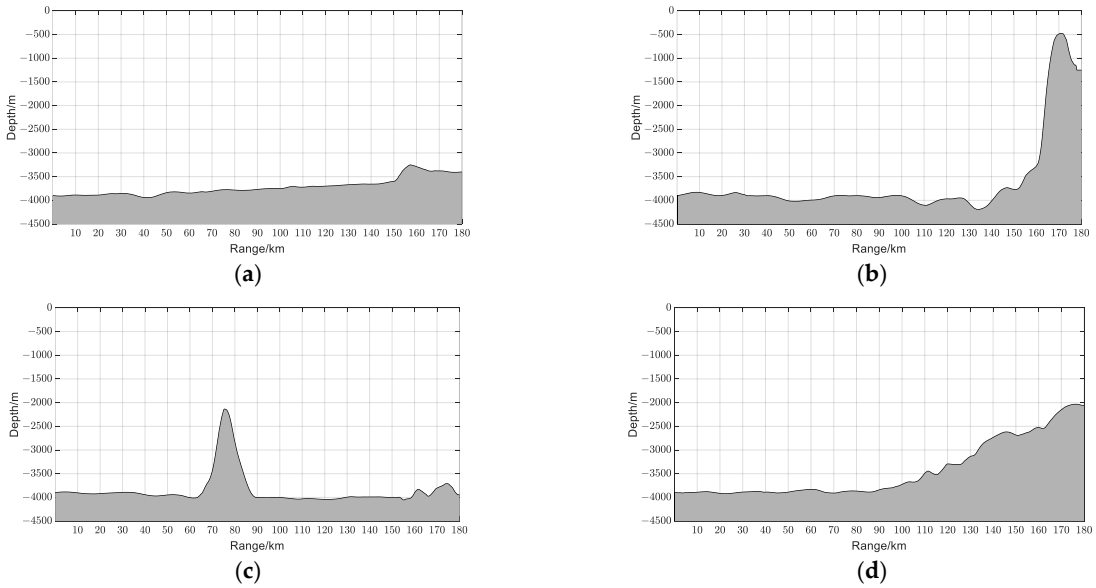

Figure 3. Water depth variation of the four acoustic survey lines at station O2. (**a**) Change in water depth of acoustic survey line O2-T1; (**b**) Change in water depth of acoustic survey line O2-T2; (**c**) Change in water depth of acoustic survey line O2-T3; (**d**) Change in water depth of acoustic survey line O2-T4.

Due to the fact that the Kuroshio intrusion in the Luzon straight almost only occurs in autumn and winter [12], the acoustic velocity profiles near stations O1 and O2 were

obtained by using the average data of Argo (ftp://data.argo.org.cn/pub/ARGO/raw_argo_data/, accessed on 12 July 2024) in autumn over the study period, as shown in Figure 4. The channel axis of station O1 is about 1000 m, and there is a surface isosonic velocity layer, while the channel axis of station O2 is also about 1000 m, but there is a surface channel with a thickness of about 45 m.

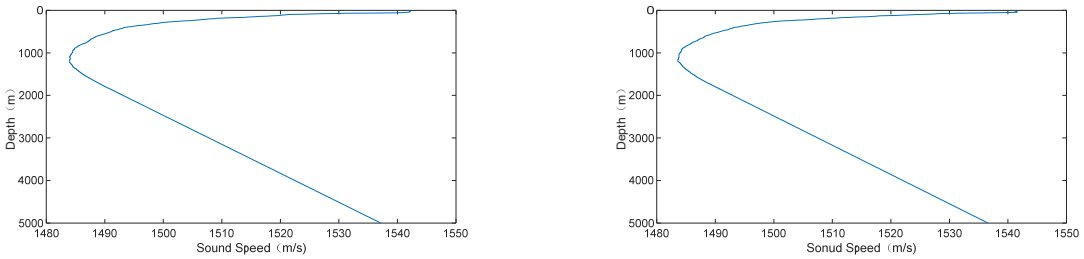

Figure 4. Acoustic velocity profiles at stations O1 and O2. (**a**) Change in the acoustic velocity profile at station O1; (**b**) Change in the acoustic velocity profile at station O2.

3. Analysis of Acoustic Transmission Characteristics

The model employed in this study is the BELLHOP ray model [13], which was proposed by Porter [14] through the introduction of the Gaussian approximation method in geoacoustics. This model has been found to better solve the influence of the acoustic field calculation on the caustics, and delivers obvious improvements in the treatment of acoustic energy caustics and the complete shadow area compared with the traditional ray model [15]; plus, it can be used for acoustic field calculation in a three-dimensional environment [16,17]. In addition, compared to the parabolic equations, normal-mode models, and wavenumber integration techniques, etc., the ray modelling is fast enough to make timely predictions that meet the requirements.

Since the medium impedance of the sea surface air is much smaller than that of seawater, the sea surface is an absolute soft boundary, and the sea bottom is set as a liquid semi-space sea bottom. According to the type of seabed substrate [18], the acoustic velocity, density, and sound absorption coefficient of the sea bottom are given in Table 1, and the range of the ray grazing angle is -90° to 90°.

Table 1. Bottom parameters for the simulation study.

c_p/(m/s)	c_s/(m/s)	α_p/(dB/λ_p)	α_s/(dB/λ_s)	ρ/(kg/m^3)
1600	0	0.5	0	1800

(1) Station O1

Figure 5 shows the transmission loss of acoustic survey line O1-S1 when the sound source frequency is 200 Hz and the sound source depth is 10, 100, 300, or 1000 m. As can be seen, when the depth of the sound source is shallow, the ray is reflected on the seabed and sea surface many times, and the transmission loss is larger. With an increase in the depth of the sound source, the number of reflections on the seabed and sea surface of the ray reduce, the transmission loss is smaller, and thus it spreads farther. When the sound source is located near the acoustic axis, the acoustic energy is mainly concentrated in the acoustic axis. When the distance is 80 km, the water depth approaches the acoustic axis depth, and the transmission of rays in the acoustic axis begins to be greatly affected by the seabed.

Figure 6 shows the transmission loss of acoustic survey line O1-S2 when the sound source frequency is 200 Hz and the sound source depth is 10, 100, 300, or 1000 m. Compared with acoustic survey line O1-S1, the water depth of O1-S2 gradually deepens, which is more suitable for long-distance transmission. When the sound source is shallow, the ray is greatly affected by the seabed after multiple seabed reflections. With an increase in

the depth of the sound source, more rays from the sound source are reversed to the sea layer and are less affected by the seabed. For example, when the depth of the sound source is 300 m, three convergence areas appear, among which the first convergence area is affected by the seabed reflection, and the second and third convergence areas are mainly formed by the ray reversal. When the sound source is located near the acoustic axis, the energy of sound transmission is concentrated in the acoustic axis, which is more suitable for long-distance transmission.

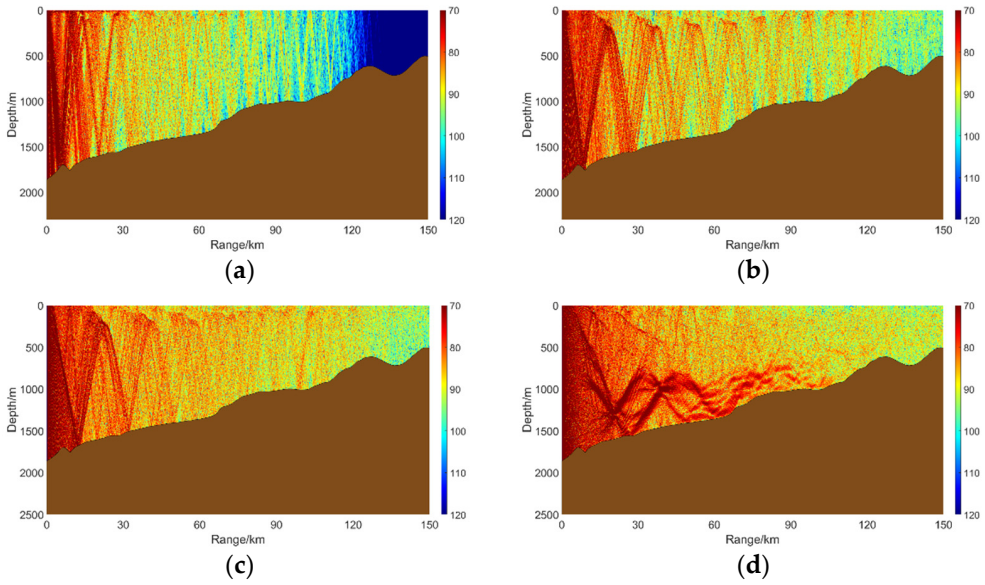

Figure 5. Transmission loss of different sound source depths of acoustic survey line O1-S1. (**a**) Transmission loss at a depth of 10 m; (**b**) Transmission loss at a depth of 100 m; (**c**) Transmission loss at a depth of 300 m; (**d**) Transmission loss at a depth of 1000 m.

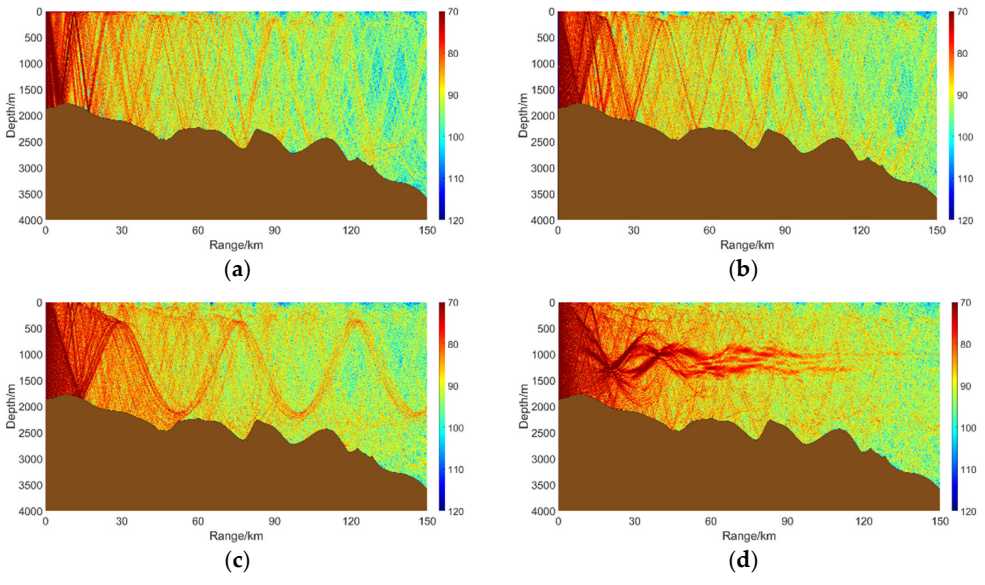

Figure 6. Transmission loss of different sound source depths of acoustic survey line O1-S2. (**a**) Transmission loss at a depth of 10 m; (**b**) Transmission loss at a depth of 100 m; (**c**) Transmission loss at a depth of 300 m; (**d**) Transmission loss at a depth of 1000 m.

Figure 7 shows the transmission loss of acoustic survey line O1-S3 when the sound source frequency is 200 Hz and the sound source depth is 10, 100, 300, or 1000 m. When the sound source is shallow, the sound line is greatly affected by the seabed after multiple

seabed reflections. With an increase in the depth of the sound source, the number of seabed reflections is reduced, and the transmission loss is smaller. When the sound source is near the acoustic axis, the acoustic energy mainly spreads within the acoustic axis.

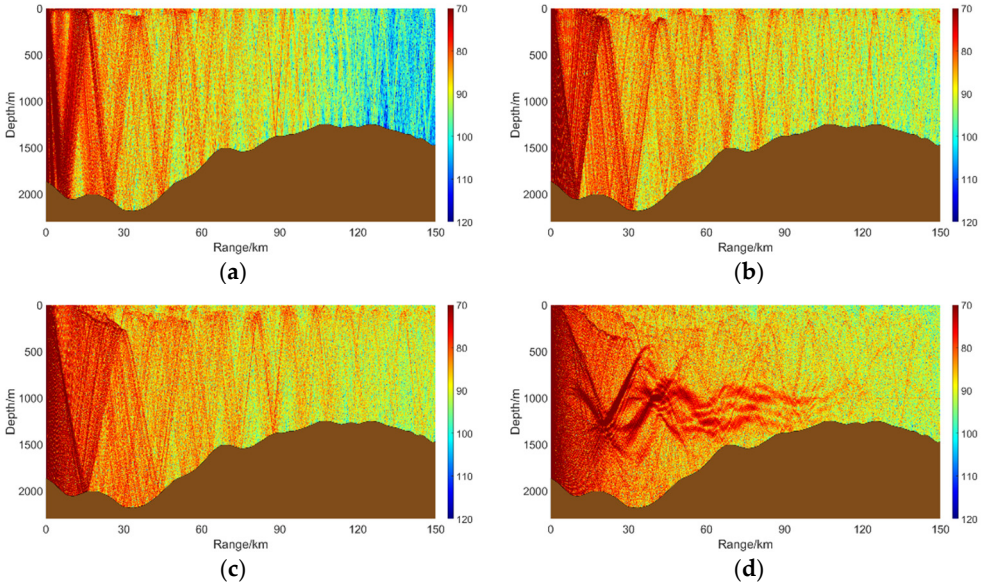

Figure 7. Transmission loss of different sound source depths of acoustic survey line O1-S3. (**a**) Transmission loss at a depth of 10 m; (**b**) Transmission loss at a depth of 100 m; (**c**) Transmission loss at a depth of 300 m; (**d**) Transmission loss at a depth of 1000 m.

Figure 8 shows the transmission loss of acoustic survey line O1-S4 when the sound source frequency is 200 Hz and the sound source depth is 10, 100, 300, or 1000 m. With an increase in the distance, the sea depth of the acoustic survey line becomes shallower from 1800 m to 150 m, and the sea depth of the acoustic survey line changes greatly. The ray passes through several sea surface and seabed reflections and is greatly affected by the seabed. When the sound source is near the acoustic axis, the transmission distance is relatively far.

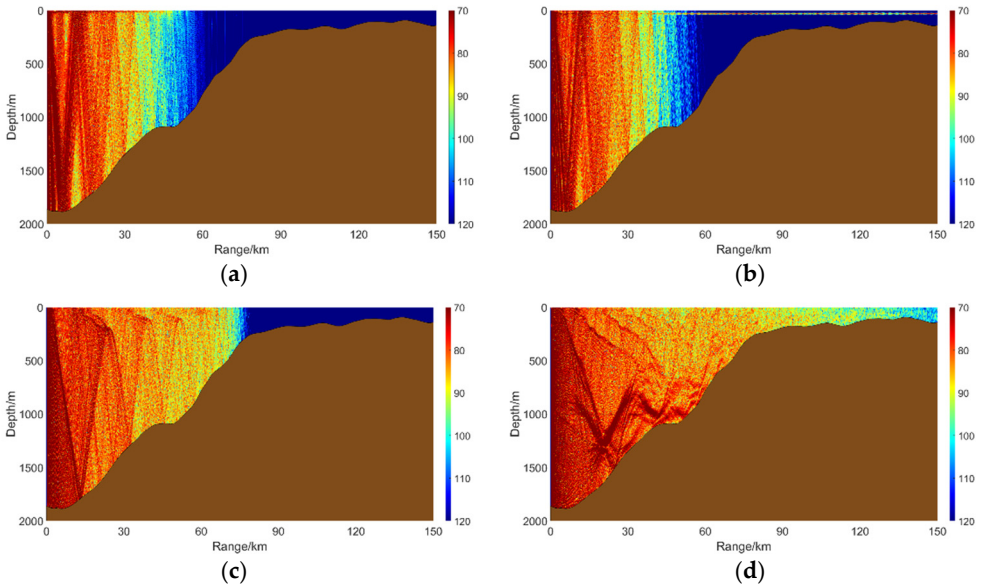

Figure 8. Transmission loss of different sound source depths of acoustic survey line O1-S4. (**a**) Transmission loss at a depth of 10 m; (**b**) Transmission loss at a depth of 100 m; (**c**) Transmission loss at a depth of 300 m; (**d**) Transmission loss at a depth of 1000 m.

(2) Station O2

Compared with the four acoustic survey lines at station O1, the average water depth of the four acoustic survey lines at station O2 is deeper, and there is a surface acoustic channel with a thickness of about 45 m.

Figure 9 shows the transmission loss of acoustic survey line O2-T1 when the sound source frequency is 200 Hz and the sound source depth is 10, 100, 300, or 1000 m. When the sound source depth is 10 m, the surface acoustic channel effect is obvious; when the sound source depth is 100 m, the ray passes through several seabed reflections and is greatly affected by the seabed; when the sound source depth is 300 m, there are three convergence areas within the range of 180 km, among which the first convergence area is about 60 km, with a width of about 20 km, the second convergence area is about 110 km, with a width of about 30 km, and the third convergence area is about 160 km, with a wider width than the first and second convergence areas. The sound shadow area is distributed between the convergence areas, and its width decreases with the increase in distance. There are also sound waves in the sound shadow area, mainly from the seabed and sea surface reflection. In general, the seabed reflection loss is larger, so the sound energy of the sound shadow area is much smaller than that of the convergence area; and when the sound source is near the sound channel axis, the sound energy is mainly concentrated near the sound channel axis.

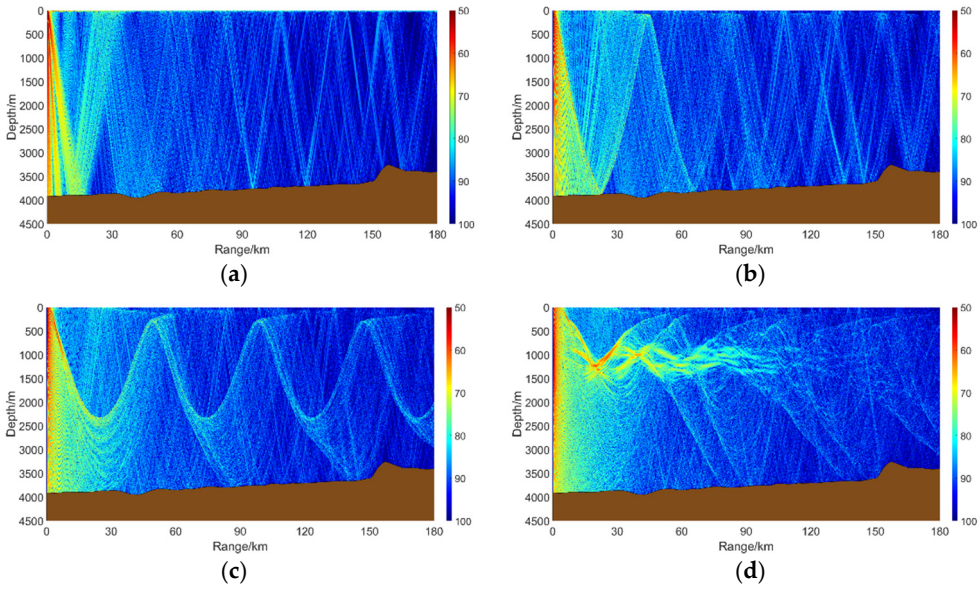

Figure 9. Transmission loss of different sound source depths of acoustic survey line O2-T1. (**a**) Transmission loss at a depth of 10 m; (**b**) Transmission loss at a depth of 100 m; (**c**) Transmission loss at a depth of 300 m; (**d**) Transmission loss at a depth of 1000 m.

Figure 10 shows the transmission loss of acoustic survey line O2-T2 when the sound source frequency is 200 Hz and the sound source depth is 10, 100, 300, or 1000 m. Except for a seamount at 160 km, the rest of the topography is similar to that of acoustic survey line O2-T1. It can also be seen that when the sound source depth is 10 m, a more obvious surface sound channel effect is presented. When the sound source depth is 100 m, the ray is reflected by the seabed many times and is greatly affected by the seabed; when the sound source depth is 300 m, there are three convergence zones within the range of 180 km; and when the sound source is located near the channel axis, the sound energy is mainly concentrated near the channel axis.

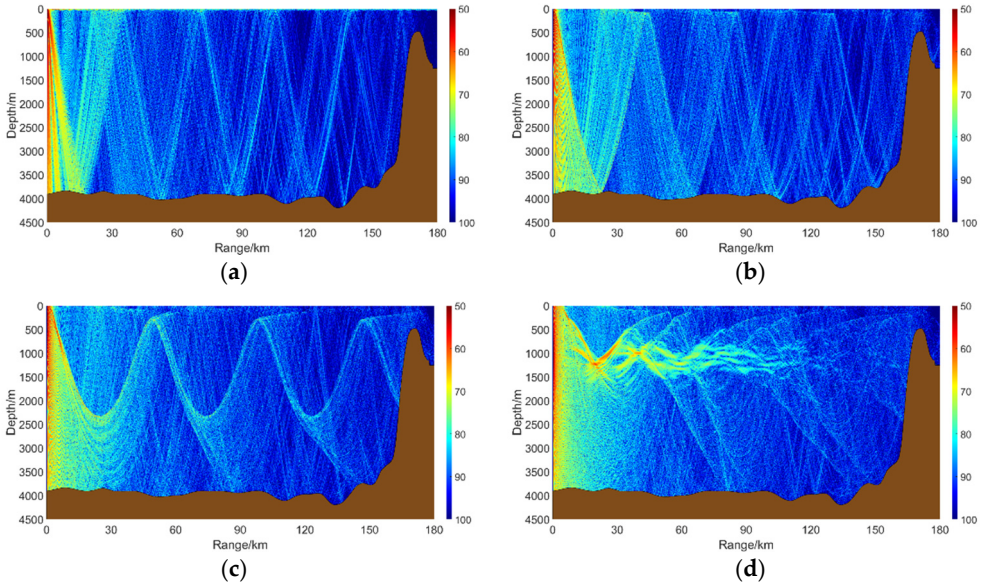

Figure 10. Transmission loss of different sound source depths of acoustic survey line O2-T2. (**a**) Transmission loss at a depth of 10 m; (**b**) Transmission loss at a depth of 100 m; (**c**) Transmission loss at a depth of 300 m; (**d**) Transmission loss at a depth of 1000 m.

Figure 11 shows the transmission loss of acoustic survey line O2-T3 when the sound source frequency is 200 Hz and the sound source depth is 10, 100, 300, or 1000 m. When the sound source depth is 10 m, there is a more obvious surface sound channel effect; when the sound source depth is 100 m, it is greatly affected by the seabed; when the sound source depth is 300, the second ray inversion near the seabed encounters the seamount, resulting in the failure to form the second and third convergence zones; and when the sound source is near the sound channel axis, the up-and-down spans of the ray inversion are small, most of the rays can avoid the seamount, and the sound transmission in the sound channel axis is less affected by the seamount.

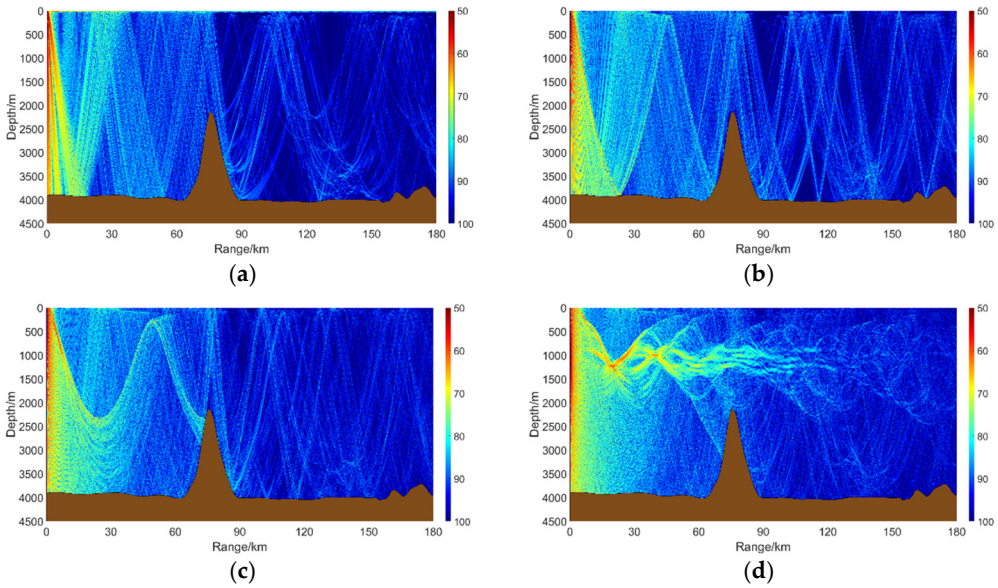

Figure 11. Transmission loss of different sound source depths of acoustic survey line O2-T3. (**a**) Transmission loss at a depth of 10 m; (**b**) Transmission loss at a depth of 100 m; (**c**) Transmission loss at a depth of 300 m; (**d**) Transmission loss at a depth of 1000 m.

Figure 12 shows the transmission loss of acoustic survey line O2-T4 when the sound source frequency is 200 Hz and the sound source depth is 10, 100, 300, or 1000 m. When the depth of the sound source is shallow, the ray is reflected by the seabed many times and is greatly affected by the seabed; then, with the increase in depth of the sound source, the ray is more reversed to the upper layer of the seawater and is less affected by the seabed. There are three convergence zones in the range of 180 km. When the sound source is near the channel axis, the upper and lower spans of the ray reversal are small and the ray mainly propagates near the channel axis.

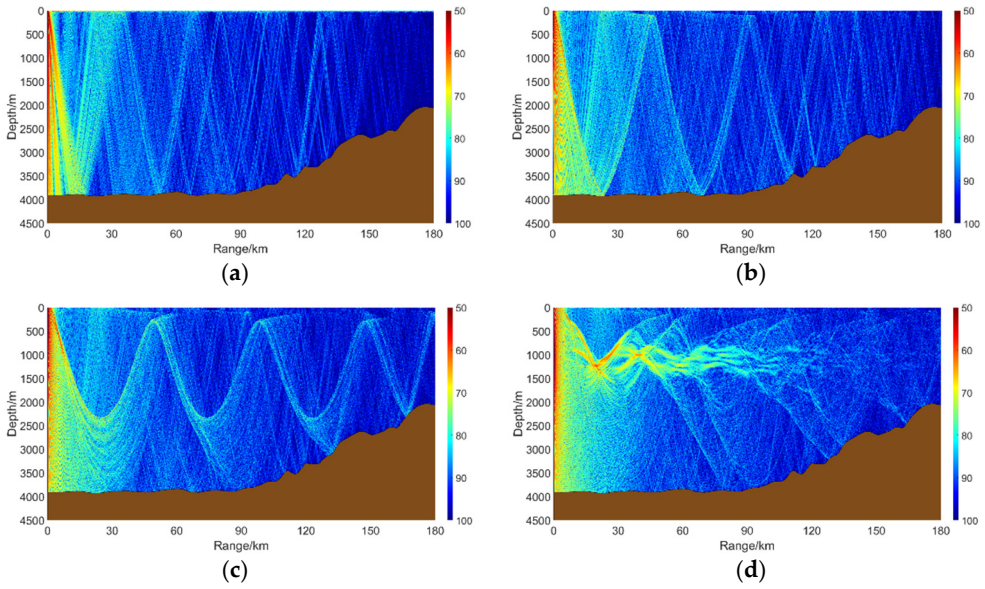

Figure 12. Transmission loss of different sound source depths of acoustic survey line O2-T4. (**a**) Transmission loss at a depth of 10 m; (**b**) Transmission loss at a depth of 100 m; (**c**) Transmission loss at a depth of 300 m; (**d**) Transmission loss at a depth of 1000 m.

4. Conclusions

In this paper, we use GEBCO_08 global topographic grid data and Argo data to numerically simulate the acoustic transmission characteristics of two stations in the northeastern part of the South China Sea. In the simulation, it is assumed that the sound velocity gradient in different propagation directions is consistent with that of the central station, and the following conclusions are obtained:

(1) When the water depth changes from deep to shallow, the number of ray reflections between the seabed and surface increases, and the transmission loss is larger. At the same time, with an increase in the sound source depth, the transmission loss is relatively small. As shown in Figures 5, 7 and 8, the water depth of the three survey lines changes from deep to shallow, and with the increase in transmission distance, the number of ray reflections between the seabed and surface increases and the transmission loss is large. It can be observed that when the depth of the sound source is increased, the transmission loss is relatively smaller.

(2) When the water depth changes from shallow to deep, the sound transmission is better than that from deep water to shallow water. As shown in Figure 6, the water depth of the survey line changes from shallow to deep, and the transmission loss is smaller than that of the transmission from deep water to shallow water in Figures 5, 7 and 8. Further comparing the propagation loss of the four different sound source depths in Figure 6, it can be seen that when the sound source depth is deeper, the propagation loss is relatively smaller. Therefore, increasing the sound source depth will also increase the propagation distance of the sound signal as the water depth changes from shallow to deep.

(3) The convergence area will greatly increase the propagation distance of sound signals. As shown in Figures 9c, 10c and 12c, in the range of 0–180 km, a total of three convergence zones appear, and the gain brought by the convergence zone can reach more than 20 dB. In actual detection, it is necessary to make full use of the convergence area to increase the propagation distance of sound signals.
(4) Terrain such as seamounts will inhibit the transmission of sound waves. As shown in Figure 11c, the second and third convergence zones cannot be formed due to the occlusion of seamounts. Therefore, when there is terrain such as seamounts, the acoustic transmission loss will increase.
(5) When there is a surface channel, the transmission of rays in the surface channel is less affected by the seabed, as shown in Figures 9a, 10a, 11a and 12a. Therefore, when the sound source is placed in the surface channel, the transmission distance will be further.
(6) Acoustic signals near the sound channel axis will propagate further. Comparing the transmission loss of the eight lines in Figures 5–12, when the sound source depth is 1000 m, close to the depth of the channel axis, the sound transmission distance is further. Therefore, when the sound source is placed near the channel axis, the transmission distance will be increased.

Author Contributions: Methodology, X.Y.; Investigation, K.Y.; Writing—original draft, X.Z.; Writing—review & editing, X.Y. All authors have read and agreed to the published version of the manuscript.

Funding: This research was funded by the National Key R&D Program of China (Grant No. 2022YFC3101901) and by the National Natural Science Foundation of China (Grant No. 52231013).

Institutional Review Board Statement: Not applicable.

Informed Consent Statement: Not applicable.

Data Availability Statement: Data are contained within the article.

Conflicts of Interest: The authors declare no conflicts of interest.

References

1. Yang, S. *Theories of Underwater Sound Propagation*; Harbin Engineering University Press: Harbin, China, 1994.
2. Jensen, F.B.; Kuperman, W.A.; Porter, M.B.; Schmidt, H.; Tolstoy, A. *Computational Ocean Acoustics*; Springer: New York, NY, USA, 2011.
3. Du, Y.; Feng, M.; Xu, Z.; Yin, B.; Hobday, A.J. Summer Marine Heatwaves in the Kuroshio-Oyashio Extension Region. *Remote Sens.* **2022**, *14*, 2980. [CrossRef]
4. Cui, W.; Yang, J.; Jia, Y.; Zhang, J. Oceanic Eddy Detection and Analysis from Satellite-Derived SSH and SST Fields in the Kuroshio Extension. *Remote Sens.* **2022**, *14*, 5776. [CrossRef]
5. Wu, C.R. Interannual modulation of the Pacific Decadal Oscillation (PDO) on the low-latitude western North Pacific. *Prog. Oceanogr.* **2013**, *110*, 49–58. [CrossRef]
6. Fang, G.; Susanto, D.; Soesilo, I.; Zheng, Q.A.; Qiao, F.; Wei, Z. A Note on the South China Sea Shallow Interocean Circulation. *Adv. Atmos. Sci.* **2005**, *22*, 946–954.
7. Stommel, H.M. *Kuroshio: Physical Aspects of the Japan Current*; University of Washington Press: Seattle, WA, USA, 1972.
8. Zeng, L.; Wang, D.; Xiu, P.; Shu, Y.; Wang, Q.; Chen, J. Decadal variation and trends in subsurface salinity from 1960 to 2012 in the northern South China Sea. In Proceedings of the 19th EGU General Assembly Conference, Vienna, Austria, 23–28 April 2017.
9. Sun, Z.; Zhang, Z.; Qiu, B.; Zhang, X.; Zhou, C.; Huang, X.; Zhao, W.; Tian, J. Three-Dimensional Structure and Interannual Variability of the Kuroshio Loop Current in the Northeastern South China Sea. *J. Phys. Oceanogr.* **2020**, *50*, 2437–2455. [CrossRef]
10. Selvaraj, M.; Choe, Y. Well ordered two-dimensional SnSBA-15 catalysts synthesized with high levels of tetrahedral tin for highly efficient and clean synthesis of nopol. *Appl. Catal. A Gen.* **2010**, *373*, 186–191. [CrossRef]
11. Hu, M.; Li, L.; Jin, T.; Jiang, W.; Wen, H.; Li, J. A New $1' \times 1'$ Global Seafloor Topography Model Predicted from Satellite Altimetric Vertical Gravity Gradient Anomaly and Ship Soundings BAT_VGG2021. *Remote Sens.* **2021**, *13*, 3515. [CrossRef]
12. Ma, C. The Variability of the Kuroshio and Its Effects on the Current in the Taiwan Strait. Master's Thesis, Ocean University of China, Qingdao, China, 2006.
13. Solgi, M.; Mahdizadeh, M.M.; Hassanzadeh, S. The effect of salt-fingering structure on sound propagation in the Strait of Hormuz. *Estuar. Coast. Shelf Sci.* **2023**, *280*, 108180. [CrossRef]

14. Porter, M.B.; Bucker, H.P. Gaussian beam tracing for computing ocean acoustic fields. *J. Acoust. Soc. Am.* **1987**, *82*, 1349–1359. [CrossRef]
15. Kumar, A.; Kumar, R.; Chandra, M.; Kishore, K. Study of under-water Sonar System for change in propagation speed, depth of water, bottom loss and estimating optimal PDFs. In Proceedings of the 2023 6th International Conference on Information Systems and Computer Networks (ISCON), Mathura, India, 3–4 March 2023; pp. 1–6.
16. Bucker, H.P. A simple 3-D Gaussian beam sound propagation model for shallow water. *J. Acoust. Soc. Am.* **1998**, *95*, 2437–2440. [CrossRef]
17. Weinberg, H.; Keenan, R.E. Gaussian ray bundles for modeling high-frequency propagation loss under shallow-water conditions. *J. Acoust. Soc. Am.* **1996**, *100*, 1421–1431. [CrossRef]
18. Hamilton, E.L. Geoacoustic modeling of the sea floor. *J. Acoust. Soc. Am.* **1980**, *68*, 1313–1340. [CrossRef]